

Original paper

# Bluelizardite, $\text{Na}_7(\text{UO}_2)(\text{SO}_4)_4\text{Cl}(\text{H}_2\text{O})_2$ , a new uranyl sulfate mineral from the Blue Lizard mine, San Juan County, Utah, USA

Jakub PLÁŠIL<sup>1\*</sup>, Anthony R. KAMPF<sup>2</sup>, Anatoly V. KASATKIN<sup>3</sup>, Joe MARTY<sup>4</sup><sup>1</sup> Institute of Physics, Academy of Sciences of the Czech Republic v.v.i, Na Slovance 2, 182 21, Prague 8, Czech Republic; [plasil@fzu.cz](mailto:plasil@fzu.cz)<sup>2</sup> Mineral Sciences Department, Natural History Museum of Los Angeles County, 900 Exposition Boulevard, Los Angeles, CA 90007, USA<sup>3</sup> V/O “Almazjuvelirexport”, Ostozhenka str., 22, block 1, 119034 Moscow, Russia<sup>4</sup> 5199 E. Silver Oak Rd., Salt Lake City, UT 84108, USA

\* Corresponding author



Bluelizardite (IMA 2013-062),  $\text{Na}_7(\text{UO}_2)(\text{SO}_4)_4\text{Cl}(\text{H}_2\text{O})_2$ , is a new uranyl sulfate mineral from the Blue Lizard mine, San Juan County, Utah (USA). It was found in a sandstone matrix and is associated with chalcantite, copiapite, ferrinatrite, gypsum, kröhnkite, johannite, and several other new, unnamed Na- and Mg-containing uranyl sulfates. Bluelizardite is a supergene mineral formed by the post-mining weathering of uraninite. The mineral is monoclinic,  $C2/c$ , with  $a = 21.1507(6)$ ,  $b = 5.3469(12)$ ,  $c = 34.6711(9)$  Å,  $\beta = 104.913(3)^\circ$ ,  $V = 3788.91(17)$  Å<sup>3</sup> and  $Z = 8$ . Crystals are blades up to 0.4 mm long, flattened on {001}, elongated parallel to [010] and exhibiting the forms {100}, {001} and {111}. Bluelizardite is pale yellow and has a yellowish-white streak. It has good cleavage on {001} and uneven fracture. The Mohs hardness is estimated at 2. The calculated density based on the empirical formula is 3.116 g/cm<sup>3</sup>. Bluelizardite exhibits bright yellow-green fluorescence under both long- and short-wave UV radiation. The mineral is optically biaxial (–), with  $\alpha = 1.515(1)$ ,  $\beta = 1.540(1)$  and  $\gamma = 1.545(1)$  (measured with white light). The measured  $2V$  is  $48(2)^\circ$  and the calculated  $2V$  is  $47.6^\circ$ . The mineral does not exhibit any dispersion or pleochroism. The optical orientation is  $X = \mathbf{b}$ ,  $Y \approx \mathbf{a}$ ,  $Z \approx \mathbf{c}^*$ . The empirical formula of bluelizardite is  $\text{Na}_{6.94}(\text{U}_{1.02}\text{O}_2)(\text{SO}_4)_{4.00}\text{Cl}_{0.94}\text{O}_{0.06}(\text{H}_2\text{O})_2$  (based on 21 anions *pfu*). The Raman spectrum is dominated by the symmetric stretching vibrations of the uranyl ( $\text{UO}_2^{2+}$ ) group and sulfate tetrahedra and by the O–H stretching and bending vibrations of the  $\text{H}_2\text{O}$  molecules. The eight strongest powder X-ray diffraction lines are [ $d_{\text{obs}}$  (Å) ( $hkl$ )]: 17.08(52)(002), 10.31(60)(200), 5.16(100)(mult.), 4.569(22)(402,–114), 4.238(23)(–115, 310, 008), 3.484(27)(–602,–604,–2·0·10), 3.353(28)(mult.), 3.186(36)(mult.). The crystal structure of bluelizardite ( $R_1 = 0.016$  for 4268 reflections with  $I_{\text{obs}} > 3\sigma I$ ) is topologically unique among known structures of uranyl minerals and inorganic compounds. It is based upon clusters of uranyl pentagonal bipyramids and sulfate tetrahedra. Two uranyl pentagonal bipyramids are linked through the two vertices of  $\text{SO}_4$  groups. The remaining three vertices of each  $\text{UO}_7$  bipyramid are occupied by  $\text{SO}_4$  groups, linked monodentately. The eight independent  $\text{Na}^+$  cations are linked through the Na–O bonds along with hydrogen bonds (involving H...O and H...Cl bonds) into a 3D framework.

**Keywords:** bluelizardite, new mineral, uranyl sulfate, weathering, crystal structure, bond-valence

**Received:** 2 November 2013; **accepted:** 22 January 2014; **handling editor:** J. Sejkora

The online version of this article (doi: 10.3190/jgeosci.159) contains supplementary electronic material.

## 1. Introduction

Uranyl sulfate minerals are important alteration products resulting from hydration–oxidation weathering of primary uranium minerals, mainly uraninite. They are not uncommon because uraninite is often associated with sulfides such as pyrite, marcasite and chalcopyrite (Finch and Murakami 1999; Krivovichev and Plášil 2013). During hydration–oxidation weathering processes, acid solutions are derived from the decomposition of sulfides under oxidizing conditions. As acid mine drainage (AMD), such solutions can transport the uranyl ion in aqua-complexes over long distances (Fernandes et al. 1995; Johnson 2003; Johnson and Hallberg 2005). Uranyl sulfate minerals form from such solutions under certain conditions (pH–Eh change, oversaturation, hydrolysis etc.) and in suitable

environments, e.g. in old mining adits with moderate relative humidity.

Bluelizardite is a new uranyl sulfate mineral found at the Blue Lizard mine, San Juan County, Utah, USA. The mineral is particularly interesting for its chemical composition, as it is a uranyl sulfate hydrate containing sodium and chlorine, and its crystal structure, which is unique among uranyl minerals. The new mineral and the name were approved by the Commission on New Minerals, Names and Classification of the International Mineralogical Association (IMA 2013-062). The new mineral was named after the type locality, the Blue Lizard mine. One holotype and three cotype specimens of bluelizardite were deposited in the collections of the Natural History Museum of Los Angeles County under the catalogue numbers 64060, 64061, 64062 and 64063.

## 2. Occurrence

Bluelizardite was found underground in the Blue Lizard mine, Red Canyon, White Canyon district, San Juan County, Utah, USA (37°33'26"N 110°17'44"W) by one of the authors (JM). The detailed description of the locality and its geological setting was provided by Kasatkin et al. (2013) and Plášil et al. (2013a). The Blue Lizard mine is the type locality for the recently described new minerals manganoblödite, cobaltoblödite (Kasatkin et al. 2013), belakovskiite (Kampf et al. 2013) and meisserite (Plášil et al. 2013a). The mineral association described here is of supergene origin, related to post-mining processes (the mine was closed in 1978), which include supergene oxidation of primary ores (uraninite, pyrite and chalcopyrite disseminated in lenses of organic matter) in the humid underground environment, which led to the formation of a variety of secondary minerals, mainly sulfates, occurring as efflorescent crusts on the surfaces of mine walls.

Minerals found in direct spatial association with bluelizardite include chalcalthite, copiapite, ferrinatriite, gypsum, johannite, kröhnkite and several new, unnamed Na- and Mg-containing uranyl sulfates. Primary minerals in the general assemblage include barite, bornite, calcite, chalcopyrite, covellite, feldspar, pyrite, quartz and uraninite. Supergene, post-mining minerals in the general assemblage include atacamite, belakovskiite, blödite, cobaltoblödite and manganoblödite, brochantite, chalcalthite, copiapite, cyanotrichite, d'ansite-(Mn), ferrinatriite, gypsum, halotrichite, johannite, meisserite, metavoltine, natrozippeite, pseudojohannite, römerite, rhomboclase, sideronatriite and tamarugite.

## 3. Physical and optical properties

Bluelizardite forms as long bladed crystals (Fig. 1) in hedgehog-like aggregates in association with other uranyl sulfate minerals. Blades are up to 0.4 mm long, flattened on {001} and elongated parallel to [010], and exhibit the forms {100}, {001} and {111} (Fig. 2). Bluelizardite is pale yellow and has a yellowish-white streak. Crystals are transparent with a vitreous luster. They are brittle, with good cleavage on {001}, and they have uneven fracture. The Mohs hardness is estimated at 2. There is insufficient material for the direct determination of density. A density of 3.116 g/cm<sup>3</sup> was calculated based on the unit-cell dimensions from single-crystal X-ray data and on the empirical formula from electron microprobe results. Bluelizardite shows bright yellow-green fluorescence under both long- and short-wave UV radiation. The mineral is optically biaxial negative, with  $\alpha = 1.515(1)$ ,  $\beta = 1.540(1)$ ,  $\gamma = 1.545(1)$  (measured in white light). The measured  $2V$  using a spindle-stage is  $48(2)^\circ$  and

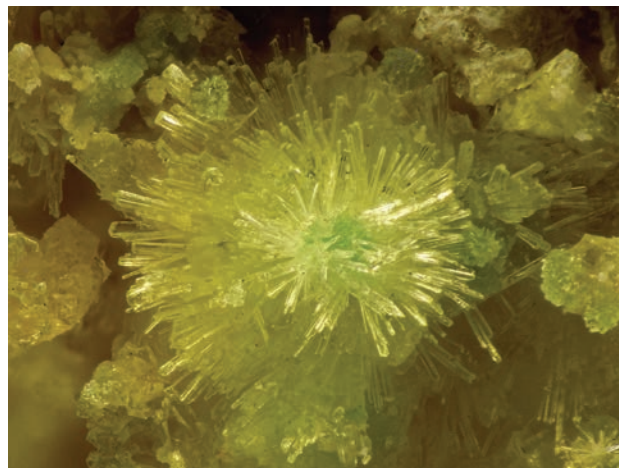


**Fig. 1** Aggregate of bluelizardite crystals. Blue Lizard mine, USA. Width of the photograph 3.5 mm (photo J. Marty).

the calculated  $2V$  is  $47.6^\circ$ . No dispersion or pleochroism was observed. The optical orientation is  $X = \mathbf{b}$ ,  $Y \approx \mathbf{a}$ ,  $Z \approx \mathbf{c}^*$ . The Gladstone-Dale compatibility,  $1 - (K_p/K_c)$ , is excellent (0.033) for the empirical formula and the single-crystal cell.

## 4. Chemical composition

The chemical composition of bluelizardite was determined using a Jeol Superprobe 733 scanning electron

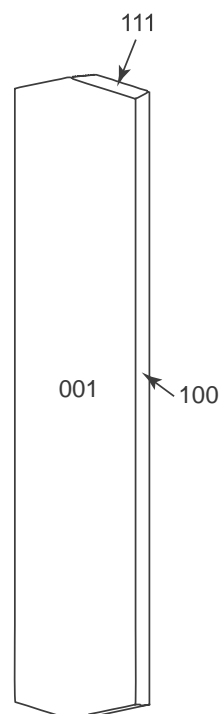


**Fig. 2** Crystal drawing of bluelizardite (clinographic projection in nonstandard orientation: [010] vertical).

**Tab. 1** Results of chemical analysis (in wt. %) of bluelizardite

	Mean ( $n = 5$ )	Range	SD	Standard
Na <sub>2</sub> O	24.15	23.40–24.55	0.47	Albite
SO <sub>3</sub>	35.84	34.70–37.45	0.99	Cu <sub>3</sub> VS <sub>4</sub>
UO <sub>3</sub>	32.89	30.45–35.14	1.76	UO <sub>2</sub>
Cl	3.76	3.46–4.01	0.22	Cs <sub>2</sub> ReCl <sub>6</sub>
H <sub>2</sub> O	4.05*			
OH = Cl	0.85			
total	99.94			

\* calculated from the structure

SD – standard deviation

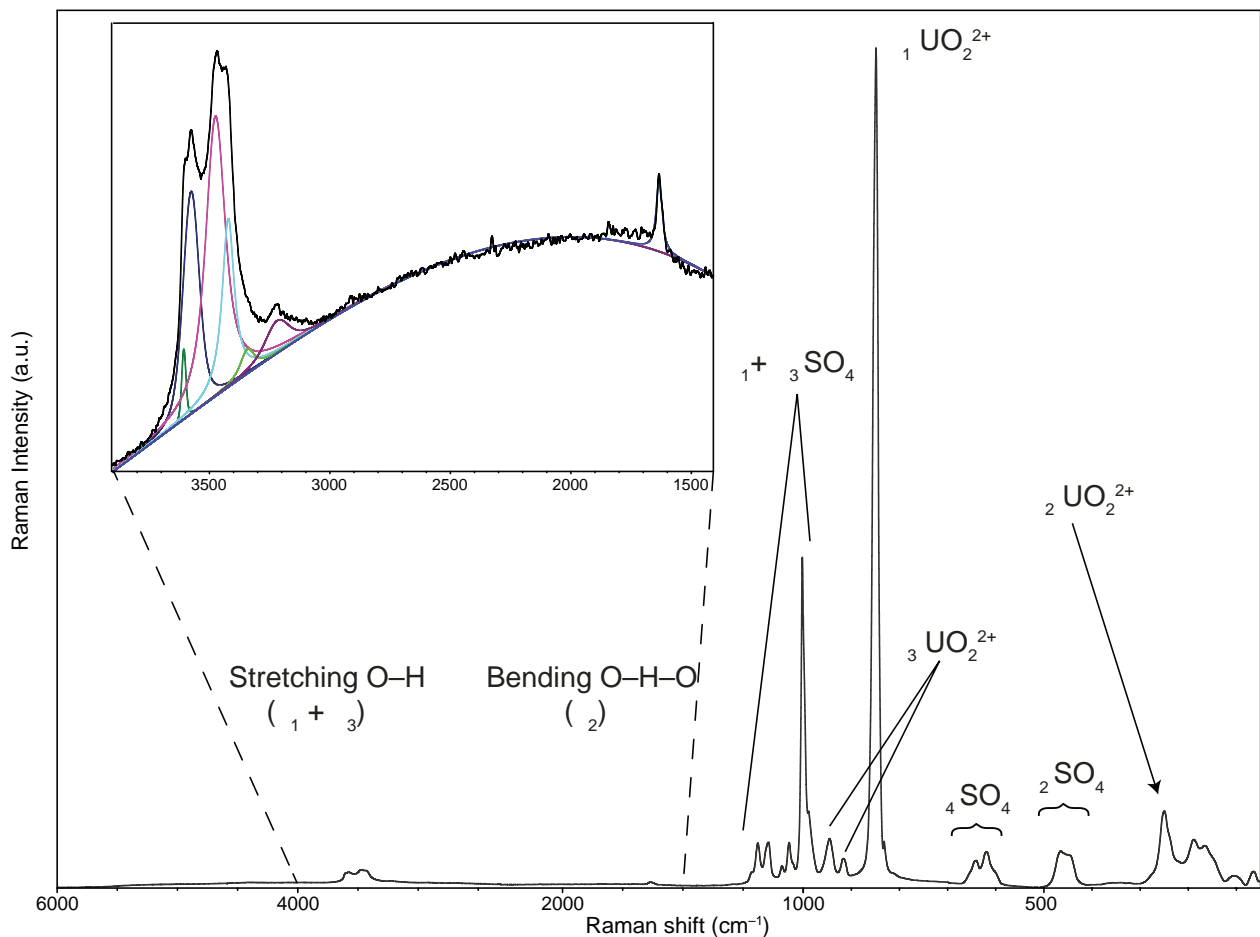
microscope (SEM) equipped with an INCA energy-dispersive X-ray spectrometer (Fersman Mineralogical Museum, Moscow). An operating voltage of 20 kV was used with a beam current of 2 nA and a 1  $\mu$ m beam diameter. The EDS mode on the SEM was chosen for the analysis instead of the WDS mode on the electron microprobe (EMP) because bluelizardite is very unstable under the higher current of the EMP beam, clearly due to its high content of easily volatilized components (Na, Cl and H<sub>2</sub>O). The content of molecular H<sub>2</sub>O was not determined directly, because of the paucity of pure material for

thermal analysis. Instead, the H<sub>2</sub>O content was calculated by stoichiometry as indicated by the crystal-structure determination.

The empirical formula of bluelizardite, calculated as the mean of 5 representative spot analyses (Tab. 1), is Na<sub>6.94</sub>(U<sub>1.02</sub>O<sub>2</sub>)(SO<sub>4</sub>)<sub>4.00</sub>Cl<sub>0.94</sub>O<sub>0.06</sub>(H<sub>2</sub>O)<sub>2</sub> (based on 21 anions *pfu*). The simplified formula, Na<sub>7</sub>(UO<sub>2</sub>)(SO<sub>4</sub>)<sub>4</sub>Cl(H<sub>2</sub>O)<sub>2</sub>, requires Na<sub>2</sub>O 24.46, UO<sub>3</sub> 32.31, SO<sub>3</sub> 36.07, Cl 4.00, H<sub>2</sub>O 4.06, O = Cl – 0.90, total 100.00 wt. %.

## 5. Raman spectroscopy

A Raman spectrum (Fig. 3) was collected using a DXR dispersive Raman spectrometer (Thermo Scientific) mounted on a confocal Olympus microscope (100 $\times$  objective). The Raman signal was excited by a 532 nm diode-pumped solid-state laser and detected by a CCD detector. The experimental parameters were: 5 s exposure time, 32 exposures, 400 lines/mm grating, 50 mm slit spectrograph aperture, and 3.0 mW laser power level. The instrument was calibrated by a software-controlled calibration procedure using multiple neon emission lines

**Fig. 3** Raman spectrum of bluelizardite.

(wavelength calibration), multiple polystyrene Raman bands (laser frequency calibration) and standardized white-light sources (intensity calibration).

Many well-documented and rigorously-assigned Raman or infrared spectra of uranyl–sulfate minerals have been published. The general features of the vibration spectra of uranyl–sulfate minerals were reviewed by Čejka (1999). Recently, the Raman spectrum of meisserite, which is structurally very similar to bluelizardite, was published (Plášil et al. 2013a). We based the assignment and interpretation of the bluelizardite Raman spectrum on the similarities with the meisserite spectrum and also on the well-resolved Raman spectrum of natural zippeite (Plášil et al. 2010).

The dominant features in the Raman spectrum of bluelizardite are U–O symmetric and S–O symmetric stretching vibrations, with expected highest intensities in the Raman (Čejka 1999; Plášil et al. 2010). The O–H vibrations, which are generally weak in un-polarized Raman spectra, are easily observable in the bluelizardite spectrum (Fig. 3).

The U–O stretching region is dominated by a sharp band at  $\sim 860\text{ cm}^{-1}$ , which is attributable to the  $\nu_1$  symmetric stretching U–O vibration of the  $(\text{UO}_2)^{2+}$  ion. Closer inspection and band-component analysis of the spectrum show that the band is composed of two overlapping vibrations at  $854$  and  $848\text{ cm}^{-1}$ . It is interesting that, in the bluelizardite spectrum, the  $\nu_3$  antisymmetric stretching U–O vibration is observable, while it is not in the meisserite spectrum (Plášil et al. 2013a). In general,  $\nu_3\text{ UO}_2^{2+}$  is not active in Raman for  $C_{\infty v}$  point symmetry; however, for bluelizardite, the symmetry of the uranyl ion is lowered by the symmetry of the U and corresponding O sites (factor-group symmetry) and forbidden modes become active. The low-intensity bands at  $918$  and  $912\text{ cm}^{-1}$  were assigned to the  $\nu_3$  antisymmetric stretching U–O vibrations. The inferred U–O uranyl bond-lengths, using the equations of Bartlett and Cooney (1989), are  $1.76\text{ \AA}$  ( $\nu_1$ ) and  $1.77\text{ \AA}$  ( $\nu_3$ ). These values perfectly match the U–O bond-lengths obtained in our refinement of the crystal structure (see below). The Raman bands at  $260$ ,  $252$ ,  $237$  and  $208\text{ cm}^{-1}$  were assigned to the  $\nu_2$  ( $\delta$ ) O–U–O bending vibrations. The number of observed bands is in agreement with there being two U atoms in the primitive unit-cell (the unit-cell of bluelizardite is C-centered).

The group of Raman bands with the second-highest intensity corresponds to the S–O symmetric stretching vibrations ( $\nu_1$ ) of  $\text{SO}_4$  tetrahedra, located at around  $\sim 1060\text{ cm}^{-1}$ . The large number of bands that can be assigned to the symmetric stretching modes (those at  $1061$ ,  $1050$ ,  $1012$ ,  $1003$ ,  $998$ ,  $986$ ,  $951$  and  $941\text{ cm}^{-1}$ ) is caused by the presence of 8 independent  $\text{SO}_4$  groups in the primitive cell. The bands at higher energy,  $1216$ ,  $1189$ ,  $1156$ ,  $1143$  and  $1090\text{ cm}^{-1}$ , were assigned to the ( $\nu_3$ ) antisymmetric

stretching vibrations of the  $\text{SO}_4$  tetrahedra. The bending modes of the  $\text{SO}_4$  groups are responsible for the Raman bands at  $651$ ,  $641$ ,  $620$  and  $619\text{ cm}^{-1}$  (triply degenerate  $\nu_4$  bending mode) and at  $607$ ,  $592\text{ cm}^{-1}$  (doubly degenerate  $\nu_2$  bending mode).

The highest-energy bands ( $\sim 3600$  to  $3200\text{ cm}^{-1}$ ) in the Raman spectrum are dominated by the O–H stretching vibrations of the  $\text{H}_2\text{O}$  molecules. Band-component analysis indicated bands at  $3606$ ,  $3576$ ,  $3475$ ,  $3422$ ,  $3343$  and  $3219\text{ cm}^{-1}$ . Using the correlation of Libowitzky (1999), it is possible to infer the approximate O...O (donor–acceptor) distances and also H...O (hydrogen–acceptor) distances for the corresponding hydrogen-bonds, based on the wavenumbers of the O–H stretching frequencies. The inferred distances from the observed frequencies for bluelizardite vary between  $2.7$  and  $3.1\text{ \AA}$  (O...O). The inferred H–A distances match the range  $1.8$  to  $2.4\text{ \AA}$ ; these numbers correspond with the bond-lengths obtained for the H-bonds from the structure refinement (see below), although the low end of the range is somewhat lower than the value from X-rays ( $\sim 1.9\text{ \AA}$ ).

The bands at the lowest frequencies are attributable to lattice modes. The Na–O stretching and Na–Cl stretching vibrations could not be assigned to Raman bands because of overlap with other fundamental vibrations.

## 6. X-ray crystallography and structure determination

### 6.1. Powder diffraction

Powder X-ray diffraction data for bluelizardite were obtained using a Rigaku R-Axis Rapid II curved imaging plate microdiffractometer utilizing monochromatized  $\text{MoK}_\alpha$  radiation (Gandolfi method). Observed powder  $d_{\text{hkl}}$  values and intensities were derived by profile fitting using JADE 2010 software. Data (in  $\text{\AA}$ ) are given in Tab. 2. Unit-cell parameters refined from the powder data using JADE 2010 with whole-pattern fitting are:  $a = 21.1822(6)$ ,  $b = 5.3544(1)$ ,  $c = 34.730(3)\text{ \AA}$ ,  $\beta = 104.879(7)^\circ$  and  $V = 3806.9(3)\text{ \AA}^3$ .

### 6.2. Single-crystal X-ray diffraction and structure solution

A single crystal of bluelizardite, with dimensions  $0.12 \times 0.03 \times 0.02\text{ mm}$ , was examined using an Oxford Diffraction Gemini single-crystal diffractometer with an Atlas CCD detector using monochromatized  $\text{MoK}_\alpha$  radiation, with a fibre-optic Mo-Enhance collimator. The unit-cell dimensions were refined from 13395 reflections by least-squares with the CrysAlisPro package (Agilent Technologies 2012). According to the single-crystal data, blueliz-

Tab. 2 Powder diffraction data for bluelizardite

$I_{\text{obs}}$	$d_{\text{obs}}$	$d_{\text{calc}}$	$I_{\text{calc}}$	$hkl$	$I_{\text{obs}}$	$d_{\text{obs}}$	$d_{\text{calc}}$	$I_{\text{calc}}$	$hkl$	$I_{\text{obs}}$	$d_{\text{obs}}$	$d_{\text{calc}}$	$I_{\text{calc}}$	$hkl$
52	17.08	16.7828	100	0 0 2										
60	10.31	10.2360	92	2 0 0	18	2.859	2.8696	6	5 1 8	7	1.924	1.9237	3	2 0 18
10	8.39	8.3914	13	0 0 4			2.8549	14	3 1 10			1.9217	2	7 1 9
9	7.56	7.5023	10	2 0 4			2.8435	8	5 1 4			1.9138	3	7 1 15
18	5.61	5.5943	18	0 0 6			2.7971	9	0 0 12			1.8781	3	6 2 11
		5.5445	12	2 0 6			2.7755	3	6 0 10	18	1.871	1.8747	6	8 2 5
		5.1801	58	1 1 0			2.7176	4	5 1 5			1.8648	4	0 0 18
100	5.16	5.1704	19	1 1 1			2.7072	4	1 1 11			1.8585	7	0 2 13
		5.1180	9	4 0 0	20	2.674	2.6813	5	3 1 11			1.8248	3	6 2 7
		5.0701	35	1 1 1			2.6772	3	0 2 0			1.8150	2	3 1 18
		5.0429	3	1 1 2			2.6687	12	0 2 1			1.8110	2	1 1 14
		4.9739	9	4 0 4			2.6438	8	0 2 2	8	1.809	1.8063	2	1 1 17
		4.8615	5	1 1 2			2.6344	3	7 1 3			1.8050	2	1 1 13
22	4.569	4.5784	8	4 0 2			2.6325	3	8 0 2			1.7920	2	1 1 18
		4.5418	18	1 1 4	18	2.619	2.6272	5	7 1 2			1.7734	4	4 2 11
		4.3772	6	4 0 6			2.6255	10	7 1 4			1.7713	2	9 1 7
		4.2852	3	1 1 4			2.5925	6	8 0 6	13	1.766	1.7695	2	7 1 17
		4.2364	7	1 1 5			2.5696	3	2 2 1			1.7655	3	5 1 14
23	4.238	4.2124	10	3 1 0			2.5590	6	8 0 0			1.7636	3	1 1 19
		4.1957	4	0 0 8			2.5217	5	3 1 12			1.7605	3	6 0 14
		4.1001	3	3 1 1	18	2.499	2.5164	3	7 1 1			1.7338	6	8 0 18
		3.9780	5	1 1 5			2.5008	3	6 0 12			1.7284	5	1 3 5
22	3.942	3.9409	8	3 1 2			2.4936	3	5 1 11			1.7193	6	1 1 18
		3.9303	14	1 1 6			2.4867	10	0 2 5	28	1.716	1.7136	2	1 1 11
		3.8537	7	3 1 5			2.4680	3	5 1 7			1.7094	2	1 3 5
		3.7512	4	4 0 8			2.4558	6	7 1 2			1.7083	6	1 2 0 10
		3.6550	6	3 1 6			2.3796	3	7 1 9			1.7063	5	1 1 19
9	3.603	3.6387	3	1 1 7			2.3490	4	5 1 8			1.6593	2	3 3 7
		3.5735	12	2 0 8	16	2.339	2.3468	6	4 2 1	10	1.656	1.6550	5	12 0 2
		3.5250	13	6 0 2			2.3375	4	0 2 7			1.6517	3	4 2 13
27	3.484	3.4887	12	6 0 4			2.3253	6	4 2 5			1.6285	3	5 3 5
		3.4636	15	2 0 10			2.3049	7	7 1 10	11	1.619	1.6261	3	5 3 1
		3.4120	18	6 0 0	5	2.233	2.2353	3	7 1 5			1.6219	2	2 2 17
		3.3697	15	4 0 6			2.2318	2	1 1 14			1.6164	3	1 0 2 9
28	3.353	3.3379	4	3 1 5			2.2269	3	7 1 11			1.5645	3	10 2 3
		3.3221	5	5 1 2			2.2194	3	2 2 7	11	1.556	1.5533	2	5 3 5
		3.3160	8	6 0 6			2.1766	4	3 1 12			1.5465	2	3 3 11
		3.3093	6	5 1 3	15	2.135	2.1481	4	9 1 5			1.5444	2	1 1 16
		3.2525	4	5 1 0			2.1439	3	4 0 16			1.5255	3	1 3 1 10
		3.2101	14	4 0 10			2.1294	3	8 0 6			1.5184	3	6 2 13
36	3.186	3.1938	5	5 1 5			2.1073	5	6 2 5	17	1.518	1.5134	2	3 1 22
		3.1876	11	6 0 2			2.0936	3	9 1 0			1.5128	2	7 3 1
		3.1757	5	5 1 1			2.0816	5	6 2 1			1.5078	2	5 3 11
		3.1615	18	1 1 8	13	2.066	2.0765	2	7 1 7			1.5057	2	2 2 19
		3.1348	6	3 1 6			2.0654	2	2 2 9			1.4745	2	0 2 19
		3.0999	8	5 1 6			2.0601	4	1 0 8	10	1.473	1.4649	2	7 3 4
13	3.079	3.0779	10	5 1 2			2.0560	2	4 2 10			1.4520	2	1 2 2 9
		3.0419	8	3 1 9			2.0433	3	9 1 9			1.4251	2	6 2 15
		2.9899	6	5 1 7			2.0323	5	4 2 7	6	1.424	1.4220	2	1 1 1 10
		2.9419	8	3 1 7			2.0124	13	0 2 11			1.4004	2	1 3 1 16
		2.9375	3	1 1 9	24	2.007	1.9982	4	7 1 8			1.3941	2	3 3 13
20	2.916	2.9043	9	1 1 10			1.9912	4	4 2 11	7	1.390	1.3904	3	10 2 9
		2.9001	12	4 0 8			1.9896	5	1 0 10			1.3810	2	5 1 20
		2.8937	5	2 0 12			1.9722	8	10 0 2					
							1.9334	3	6 0 12					

\* Calculated lines with intensities less than 3 are not included unless they correspond to observed lines

**Tab. 3** Crystallographic data and refinement details for blueizardite

<b>Crystal data</b>	
Formula	Na <sub>7</sub> (UO <sub>2</sub> )(SO <sub>4</sub> ) <sub>4</sub> Cl(H <sub>2</sub> O) <sub>2</sub>
Crystal system	monoclinic
Space group	C2/c
Unit-cell parameters: <i>a</i> , <i>b</i> , <i>c</i> [Å]	21.1507(6), 5.3469(12), 34.6711(9)
β [°]	104.913(3)
Unit-cell volume [Å <sup>3</sup> ]	3788.91(17)
Z	8
Calculated density [g/cm <sup>3</sup> ]	3.108
Crystal size [mm <sup>3</sup> ]	0.12 × 0.03 × 0.02
<b>Data collection</b>	
Diffractometer	Oxford Diffraction Gemini with Atlas detector
Temperature [K]	320
Radiation, wavelength [Å]	MoK <sub>α</sub> , 0.71073 (50 kV, 30 mA)
θ range for data collection [°]	3.50–29.40
Limiting Miller indices	<i>h</i> = 25 → 26, <i>k</i> = 7 → 7, <i>l</i> = 46 → 43
Axis, frame width (°), time per frame (s)	ω, 0.5, 130
Total reflections collected	24440
Unique reflections	4715
Unique observed reflections, criterion	4268, [ <i>I</i> > 3σ( <i>I</i> )]
Absorption coefficient [mm <sup>-1</sup> ], type	9.41; multi-scan
<i>T</i> <sub>min</sub> / <i>T</i> <sub>max</sub>	0.514/1
Data completeness to θ <sub>max</sub> (%), <i>R</i> <sub>int</sub>	99.47, 0.025
<b>Structure refinement by Jana2006</b>	
Number of refined parameters, restraints, constraints	312, 6, 4
Data/restraints/parameters	4268/6/312
<i>R</i> <sub>1</sub> , <i>wR</i> <sub>2</sub> (obs)	0.0163, 0.0383
<i>R</i> <sub>1</sub> , <i>wR</i> <sub>2</sub> (all)	0.0205, 0.0398
GOF obs/all	1.17, 1.15
Weighting scheme, weights	σ, <i>w</i> = 1/(σ <sup>2</sup> ( <i>I</i> ) + 0.0004 <sup>2</sup> )
Largest diffraction peak and hole (e <sup>-</sup> /Å <sup>3</sup> )	0.70, -0.86

ardite is monoclinic with *a* = 21.1507(6), *b* = 5.3469(12), *c* = 34.6711(9) Å, β = 104.913(3)°, *V* = 3788.91(17) Å<sup>3</sup> and *Z* = 8. Of the 24,440 measured reflections, 4715 were independent and 4268 were classified as observed based on the criterion [*I*<sub>obs</sub> > 3σ(*I*)]. Data were corrected for Lorentz effect, polarization factor and background. An empirical (multi-scan) correction for absorption was applied to the dataset using the ABSPACK3 algorithm implemented in the RED routine of the CrysAlis software (Agilent Technologies 2012), leading to *R*<sub>int</sub> of 0.0250. Other details of the data collection are given in Tab. 3.

The crystal structure of blueizardite was solved by the charge-flipping algorithm (Oszlányi and Sütö 2004, 2008; Palatinus 2013) implemented in the Superflip program (Palatinus and Chapuis 2007) and subsequently refined using the software Jana2006 (Petříček et al. 2006) with the full-matrix least-squares refinement based on *F*<sup>2</sup>. The reflection conditions and statistics clearly indicated the monoclinic space group *C2/c*. This space group was also suggested by the Superflip program, based on the symme-

try operators deduced from the flipped electron-density (Palatinus and van der Lee 2008). All atoms except hydrogen were refined using harmonic atomic-displacement parameters. Hydrogen atoms, which were located in the difference-Fourier maps, were treated using soft constraints on bond lengths, 0.90 Å, with a constraint weight of (0.02), resulting in donor-hydrogen lengths of 0.87(3) Å, and their isotropic-displacement parameters were set to 1.2 × *U*<sub>eq</sub> of the donor O atoms. The refinement converged smoothly with final indices of agreement *R*<sub>1</sub> = 0.0163 and *wR*<sub>2</sub> = 0.0383 for 4715 observed reflections with GOF = 1.17 (Tab. 2). The atom coordinates and the displacement parameters are given in Tab. 4 and selected interatomic distances in Tabs 5 and 6. Bond-valences are presented in Tab. 7.

### 6.3. Description of the crystal structure

The asymmetric unit of the blueizardite structure contains one U site, four S sites, eight Na sites, twenty O sites (including two positions occupied by O atoms of H<sub>2</sub>O molecules) one Cl site and four H sites (Tab. 4). The U atom is strongly bonded to two O atoms (O<sub>Ur</sub>), forming a nearly linear uranyl ion, UO<sub>2</sub><sup>2+</sup>. It is further coordinated by five O atoms (O<sub>ligand</sub>) arranged as equatorial vertices of a pentagonal uranyl bipyramid with O<sub>Ur</sub> at the two vertical apices. The U–O<sub>Ur</sub> and U–O<sub>ligand</sub> bond-lengths (Tab. 5) closely match the typical values for [7]-coordinated U atoms provided by Burns et al. (1997). Uranyl pentagonal bipyramids form clusters in which two uranyl bipyramids are bridged by sharing vertices of two sulfate tetrahedra, and three additional SO<sub>4</sub> groups are linked monodentately to each bipyramid, resulting in dimers of composition [(UO<sub>2</sub>)<sub>2</sub>(SO<sub>4</sub>)<sub>8</sub>]<sup>12-</sup> (Fig. 4). The Na<sub>φ<sub>n</sub></sub> polyhedra are located between the uranyl sulfate clusters and link them into sheets stacked perpendicular to [010]; adjacent sheets (a short periodicity with the *b* = 5.35 Å) link through a dense network of Na–O and Na–Cl bonds into a three-dimensional framework (Fig. 4). Additional linkage is provided through hydrogen bonds from H<sub>2</sub>O

Tab. 4 Atom coordinates and displacement parameters for the crystal structure of bluelizardite

Atom	$x/a$	$y/b$	$z/c$	$U_{eq}$	$U^{11}$	$U^{22}$	$U^{33}$	$U^{12}$	$U^{13}$	$U^{23}$
U	0.519790(4)	0.889263(17)	0.666875(3)	0.00965(3)	0.01006(6)	0.01104(5)	0.00808(5)	0.00043(4)	0.00274(4)	0.00091(3)
S1	0.39880(3)	0.82919(12)	0.725237(18)	0.01116(19)	0.0104(3)	0.0136(3)	0.0095(3)	-0.0013(2)	0.0025(2)	0.0007(2)
S2	0.19437(3)	0.38979(12)	0.679982(19)	0.0128(2)	0.0105(3)	0.0145(3)	0.0135(3)	0.0001(2)	0.0031(2)	-0.0010(2)
S3	0.35667(3)	0.93456(12)	0.605180(19)	0.0124(2)	0.0113(3)	0.0149(3)	0.0112(3)	0.0011(2)	0.0033(2)	0.0001(2)
S4	0.52816(3)	0.97992(12)	0.565139(18)	0.01085(19)	0.0133(3)	0.0110(3)	0.0089(3)	-0.0004(2)	0.0039(2)	0.0001(2)
Na1	0.5	0.5	0.5	0.0168(5)	0.0311(9)	0.0102(7)	0.0121(7)	-0.0020(6)	0.0112(6)	-0.0005(6)
Na2	0.5	0.3688(3)	0.75	0.0261(6)	0.0300(10)	0.0226(9)	0.0248(9)	0	0.0054(7)	0
Na3	0.24344(6)	0.8755(2)	0.66014(4)	0.0236(4)	0.0224(7)	0.0245(6)	0.0246(6)	-0.0006(5)	0.0074(5)	0.0038(5)
Na4	0.31919(7)	0.4131(2)	0.75567(4)	0.0293(4)	0.0437(8)	0.0263(7)	0.0207(6)	-0.0127(5)	0.0131(6)	0.0016(5)
Na5	0.37872(6)	0.9872(2)	0.50389(3)	0.0213(4)	0.0293(7)	0.0177(6)	0.0180(6)	-0.0013(5)	0.0080(5)	-0.0009(5)
Na6	0.69460(6)	0.7427(2)	0.58061(3)	0.0273(4)	0.0294(7)	0.0288(7)	0.0214(6)	0.0031(5)	0.0022(5)	0.0034(5)
Na7	0.43332(6)	0.4189(2)	0.57801(4)	0.0230(4)	0.0263(7)	0.0214(6)	0.0241(6)	-0.0028(5)	0.0116(5)	-0.0050(5)
Na8	0.34817(6)	0.3812(2)	0.65853(4)	0.0268(4)	0.0345(8)	0.0218(6)	0.0268(7)	-0.0015(5)	0.0127(5)	-0.0057(5)
Cl	0.35728(4)	1.49234(14)	0.49530(2)	0.0255(2)	0.0335(4)	0.0164(3)	0.0239(4)	0.0010(3)	0.0025(3)	-0.0008(3)
O1	0.39670(10)	1.1009(3)	0.72350(6)	0.0211(7)	0.0297(12)	0.0148(10)	0.0184(10)	-0.0010(8)	0.0055(9)	0.0011(8)
O2	0.45053(9)	0.7322(4)	0.70702(6)	0.0211(7)	0.0185(11)	0.0287(12)	0.0198(10)	0.0068(9)	0.0118(8)	0.0065(9)
O3	0.33715(9)	0.7135(4)	0.70406(6)	0.0187(6)	0.0125(10)	0.0238(11)	0.0170(10)	-0.0047(8)	-0.0016(8)	-0.0006(8)
O4	0.41507(9)	0.7338(3)	0.76693(5)	0.0161(6)	0.0198(11)	0.0188(10)	0.0089(9)	-0.0037(8)	0.0024(7)	0.0015(7)
O5	0.19330(11)	0.6255(4)	0.70048(7)	0.0263(8)	0.0339(13)	0.0214(12)	0.0289(12)	-0.0050(9)	0.0179(10)	-0.0105(9)
O6	0.22590(10)	0.4217(4)	0.64714(6)	0.0204(7)	0.0173(11)	0.0269(11)	0.0199(10)	-0.0033(8)	0.0102(8)	-0.0073(8)
O7	0.22999(10)	0.1999(4)	0.70751(6)	0.0290(7)	0.0221(12)	0.0300(12)	0.0303(12)	0.0055(9)	-0.0016(9)	0.0109(10)
O8	0.12656(9)	0.2995(4)	0.66314(6)	0.0206(6)	0.0115(10)	0.0324(11)	0.0180(10)	-0.0028(8)	0.0040(8)	-0.0050(9)
O9	0.29776(9)	1.0279(4)	0.61533(6)	0.0199(7)	0.0126(10)	0.0238(11)	0.0247(11)	0.0036(8)	0.0074(8)	-0.0014(9)
O10	0.36035(11)	1.0275(4)	0.56665(6)	0.0259(7)	0.0320(13)	0.0344(12)	0.0130(10)	-0.0002(10)	0.0089(9)	0.0029(9)
O11	0.36047(10)	0.6618(4)	0.60765(6)	0.0221(7)	0.0220(11)	0.0146(10)	0.0296(11)	-0.0001(8)	0.0068(9)	-0.0033(9)
O12	0.41380(9)	1.0459(3)	0.63616(6)	0.0167(6)	0.0125(10)	0.0177(10)	0.0179(10)	0.0013(8)	0.0001(7)	-0.0017(8)
O13	0.50291(10)	0.7262(4)	0.5835(6)	0.0218(7)	0.0319(12)	0.0146(10)	0.0214(10)	-0.0092(9)	0.0113(9)	-0.0045(8)
O14	0.48627(10)	1.1551(4)	0.53732(6)	0.0189(6)	0.0208(11)	0.0213(10)	0.0137(9)	0.0033(8)	0.0031(8)	0.0056(8)
O15	0.59554(9)	0.9962(4)	0.56187(6)	0.0193(7)	0.0134(10)	0.0244(11)	0.0223(10)	-0.0018(8)	0.0086(8)	-0.0013(9)
O16	0.52671(9)	1.0643(3)	0.60633(5)	0.0156(6)	0.0219(11)	0.0159(10)	0.0102(9)	-0.0020(8)	0.0066(8)	-0.0022(7)
O17	0.50283(9)	0.5996(3)	0.64233(6)	0.0160(6)	0.0176(11)	0.0141(10)	0.0160(9)	0.0000(7)	0.0041(8)	-0.0004(7)
O18	0.53365(10)	1.1801(4)	0.69168(5)	0.0176(6)	0.0242(11)	0.0128(9)	0.0146(9)	-0.0001(8)	0.0031(8)	-0.0019(8)
Ow19	0.64780(11)	0.4223(4)	0.60943(7)	0.0264(8)	0.0215(12)	0.0230(12)	0.0336(13)	-0.0033(9)	0.0053(9)	-0.0073(9)
Ow20	0.23476(12)	0.5150(5)	0.53951(8)	0.0400(10)	0.0290(15)	0.0399(15)	0.0517(16)	-0.0091(12)	0.0113(12)	-0.0017(13)
H1	0.6169(11)	0.483(5)	0.6193(9)	0.0316*						
H2	0.2691(13)	0.463(5)	0.5323(12)	0.048*						
H3	0.2391(15)	0.674(4)	0.5454(12)	0.048*						
H4	0.6332(12)	0.290(5)	0.5952(9)	0.0316*						

**Tab. 5** Selected interatomic distances (Å) and angles (°) in blue lizardite

U–O17	1.7590(17)	S1–O1	1.4542(17)	S3–O9	1.467(2)
U–O18	1.765(2)	S1–O2	1.490(2)	S3–O10	1.446(2)
U–O2	2.416(2)	S1–O3	1.4592(19)	S3–O11	1.462(2)
U–O4 <sup>v</sup>	2.4958(16)	S1–O4	1.4872(6)	S3–O12	1.5164(18)
U–O8 <sup>xi</sup>	2.345(2)	<S1–O>	1.473	<S2–O>	1.473
U–O12	2.3732(17)				
U–O16	2.3371(18)	S2–O5	1.450(2)	S4–O13	1.455(2)
<U–O <sub>ur</sub> >	1.762	S2–O6	1.470(2)	S4–O14	1.467(2)
<U–O <sub>eq</sub> >	2.393	S2–O7	1.463(2)	S4–O15	1.461(2)
		S2–O8	1.4834(19)	S4–O16	1.5055(19)
		<S2–O>	1.467	<S4–O>	1.472
Na1–O13	2.344(2)	Na2–O1 <sup>i</sup>	2.576(2)	Na3–O3	2.333(2)
Na1–O13 <sup>iii</sup>	2.344(2)	Na2–O1 <sup>iv</sup>	2.576(2)	Na3–O5	2.373(3)
Na1–O14 <sup>i</sup>	2.313(2)	Na2–O2	2.507(2)	Na3–O6	2.478(2)
Na1–O14 <sup>ii</sup>	2.313(2)	Na2–O2 <sup>v</sup>	2.507(2)	Na3–O6 <sup>vi</sup>	2.964(2)
<Na1–O>	2.329	Na2–O4	2.815(2)	Na3–O7 <sup>vi</sup>	2.455(3)
Na1–Cl <sup>i</sup>	2.9811(9)	Na2–O4 <sup>v</sup>	2.815(2)	Na3–O9	2.306(3)
Na1–Cl <sup>ii</sup>	2.9811(9)	Na2–O18 <sup>i</sup>	2.520(2)	Na3–Ow19 <sup>vii</sup>	2.327(2)
		Na2–O18 <sup>iv</sup>	2.520(2)	<Na3–O>	2.462
		<Na2–O>	2.605		
Na4–O1 <sup>i</sup>	2.768(3)	Na5–O10	2.316(3)	Na6–O6 <sup>xi</sup>	2.427(2)
Na4–O3	2.505(3)	Na5–O14	2.443(2)	Na6–O9 <sup>xiii</sup>	2.485(2)
Na4–O4	2.607(2)	Na5–O15 <sup>ii</sup>	2.479(3)	Na6–O15	2.439(2)
Na4–O5 <sup>viii</sup>	2.225(3)	Na5–Ow20 <sup>x</sup>	2.484(2)	Na6–Ow19	2.329(3)
Na4–O7	2.455(2)	<Na5–O>	2.431	Na6–Ow20 <sup>xi</sup>	2.345(3)
Na4–O7 <sup>ix</sup>	2.397(3)	Na5–Cl <sup>i</sup>	2.6883(12)	<Na6–O>	2.405
<Na4–O>	2.493	Na5–Cl	2.7420(12)	Na6–Cl <sup>ii</sup>	2.8676(12)
		<Na5–Cl>	2.715		
Na7–O10 <sup>i</sup>	2.569(2)			Na8–O1 <sup>i</sup>	2.680(2)
Na7–O11	2.435(3)			Na8–O3	2.427(3)
Na7–O12 <sup>i</sup>	2.940(2)			Na8–O6	2.523(2)
Na7–O13	2.418(3)			Na8–O9 <sup>i</sup>	2.475(2)
Na7–O14 <sup>i</sup>	2.460(3)			Na8–O11	2.381(3)
Na7–O16 <sup>i</sup>	2.732(2)			Na8–O12 <sup>i</sup>	2.509(2)
Na7–O17	2.526(2)			<Na8–O>	2.499
<Na7–O>	2.583				
Na7–Cl <sup>i</sup>	2.9309(13)				
O1–O2	2.417(3)	O5–O8	2.401(3)	O11–O17	2.959(3)
O1–O3	2.428(3)	O6–O7	2.388(3)	O12–O16	2.838(3)
O1–O4	2.443(2)	O6–O8	2.398(3)	O12–O18	2.851(2)
O1–O18 <sup>v</sup>	2.961(2)	O6–O9 <sup>i</sup>	2.970(3)	O13–O14	2.405(3)
O2–O3	2.376(3)	O7–O8	2.388(3)	O13–O15	2.411(3)
O2–O4	2.383(3)	O8–O16 <sup>xiii</sup>	2.864(2)	O13–O16	2.420(3)
O2–O4 <sup>v</sup>	2.752(3)	O8–O17 <sup>xiii</sup>	2.746(3)	O13–O17	2.990(3)
O2–O12	2.911(3)	O8–Ow19 <sup>xiii</sup>	2.858(3)	O14–O15	2.403(3)
O2–O17	2.834(3)	O9–O10	2.399(3)	O14–O16	2.375(3)
O3–O4	2.373(2)	O9–O11	2.418(3)	O15–O16	2.405(3)
O4–O8 <sup>ix</sup>	2.806(3)	O9–O12	2.375(3)	O15–Ow19 <sup>vi</sup>	2.862(3)
O4–O18 <sup>v</sup>	2.851(3)	O10–O11	2.417(3)	O16–O17	2.883(2)
O5–O6	2.396(3)	O10–O12	2.386(3)	O16–O18	2.990(3)
O5–O7	2.396(3)	O11–O12	2.427(3)	O17–O18 <sup>i</sup>	2.794(3)

Symmetry codes: (i)  $x, y-1, z$ ; (ii)  $-x+1, -y+2, -z+1$ ; (iii)  $-x+1, -y+1, -z+1$ ; (iv)  $-x+1, y-1, -z+3/2$ ; (v)  $-x+1, y, -z+3/2$ ; (vi)  $x, y+1, z$ ; (vii)  $x-1/2, y+1/2, z$ ; (viii)  $-x+1/2, y-1/2, -z+3/2$ ; (ix)  $-x+1/2, y+1/2, -z+3/2$ ; (x)  $-x+1/2, -y+3/2, -z+1$ ; (xi)  $x+1/2, y+1/2, z$ ; (xii)  $x+1/2, y-1/2, z$ ; (xiii)  $-x+1/2, -y+5/2, -z+1$ ; (xiv)  $x-1/2, y-1/2, z$ .

molecules to O atoms (O8, O15) and Cl atoms (Tab. 6, Fig. 5).

## 7. Discussion

### 7.1. Structure topology and related structures

The blue lizardite structure contains  $[(\text{UO}_2)_2(\text{SO}_4)_8]^{4-}$  uranyl sulfate clusters (Fig. 6a); in contrast, the structure of meisserite (Plášil et al. 2013a), another Na-uranyl sulfate from the same locality, is based on uranyl sulfate chains (Fig. 6b). In the blue lizardite structure, the bridging sulfate tetrahedra between two uranyl pentagonal bipyramids are oriented *down* and *down*, or *up* and *up* (Fig. 6a) with respect to the plane of the sheets, whereas in meisserite, the  $\text{SO}_4$  groups that link the chains are oriented *up* and *down* (Fig. 6b). The similar infinite chain as in meisserite occurs in the structure of synthetic  $\text{Na}_3\text{Ti}_5[(\text{UO}_2)(\text{MoO}_4)_3]_2(\text{H}_2\text{O})_3$  (Krivovichev and Burns 2003). While the blue lizardite structure is characterized by two-membered clusters, the meisserite structure is characterized by chains, and the structure of belakovskiiite (Kampf et al. 2013) is based on clusters of composition  $[(\text{UO}_2)(\text{SO}_4)_4]^{6-}$  (Fig. 6c). The two-membered clusters topologically similar to these found in blue lizardite were observed in the structures of the synthetic compounds:  $\text{Na}_6[(\text{UO}_2)(\text{MoO}_4)_4]$  (Krivovichev and Burns 2001) and  $\text{Na}_3\text{Ti}_3[(\text{UO}_2)(\text{MoO}_4)_4]$  (Krivovichev and Burns 2003). Uranyl sulfate clusters of the same stoichiometry as in blue lizardite occur in synthetic compounds (Burns and Hayden 2002; Hayden and Burns 2002a, b). However, these compounds

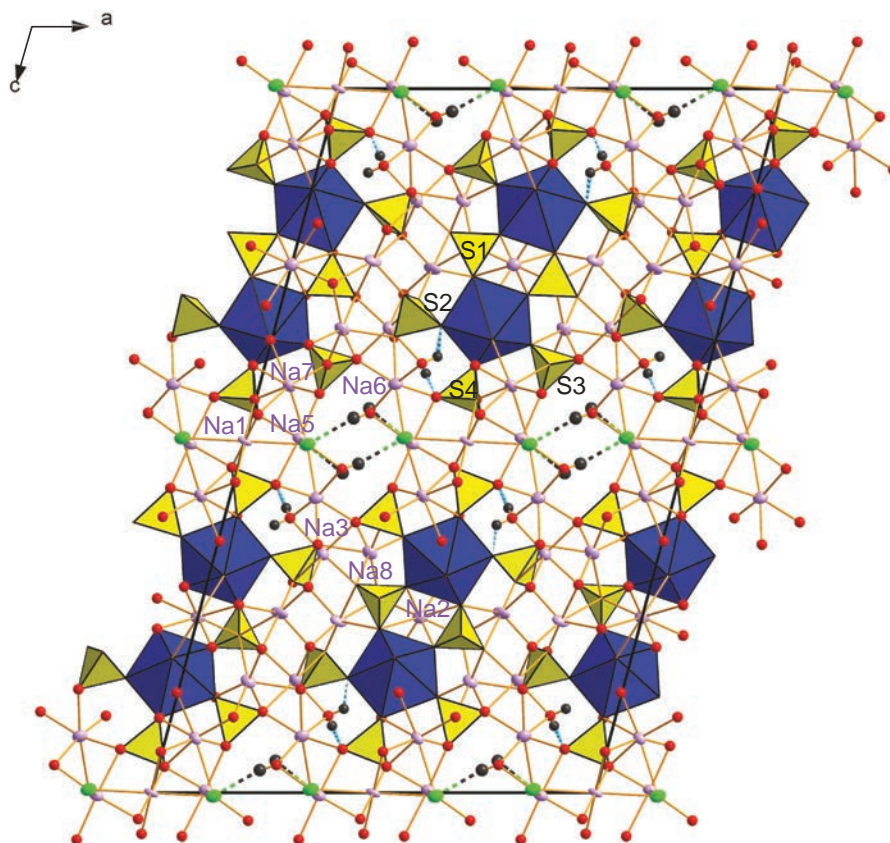


**Fig. 4** Crystal structure of bluelizardite viewed along [010].  $[(\text{UO}_2)_2(\text{SO}_4)_8]^{12-}$  clusters (U-polyhedra are blue,  $\text{SO}_4$  groups yellow) are linked into a 3D framework through Na–O (Na atoms are pink) and Na–Cl bonds (Cl atoms are green). Atoms labelled Ow19 and Ow20 are  $\text{H}_2\text{O}$  molecules, H atoms are shown in black color, O–H...O bonds are blue dashed, O–H...Cl bonds are two-colored dashed lines.

are topological isomers, as they contain a bidentately linked  $\text{SO}_4$  group (Figs 6d–f). A very similar cluster to that in bluelizardite occurs in the structure of the high-temperature synthetic compound  $\text{K}_4[(\text{UO}_2)(\text{SO}_4)_3]$  (Mikhailov et al. 1977). This structure, however, contains two bidentately linked  $\text{SO}_4$  groups (Fig. 6g).

## 7.2. Notes on origin

Bluelizardite is a uranyl sulfate mineral found in a sandstone matrix together with a diverse suite of other sulfate minerals of supergene origin. They formed from low-temperature,  $\text{SO}_4$ -bearing, acidic aqueous solutions, which can be linked to acid-mine drainage (AMD) waters originating from the dissolution of hypogene sulfide minerals (Fernandes et al. 1995; Johnson 2003; Johnson and Hallberg 2005). The occurrences of such mineral-rich alteration assemblages, including uranyl sulfates related in origin to AMD processes, are widespread (Ondruš et

al. 1997, 2003; Brugger et al. 2003, 2006; Plášil et al. 2011a, b, 2012, 2013a, b). At the Blue Lizard mine, the mineral assemblage is inferred to have formed at very low pH. Although we did not sample the mine waters at the site or measure their pH, we can draw some conclusions concerning the pH based on the known thermodynamic properties of selected minerals in the association (e.g., Majzlan 2010 and references therein; Grevel and Majzlan 2011) and from the bond-valence approach (Schindler et al. 2006; Hawthorne and Schindler 2008; Schindler and Hawthorne 2008; Hawthorne 2012). Minerals that are very characteristic of this weathering association, including römerite, rhomboclase and copiapite, are predicted to form under very low pH and at moderately oxidizing conditions (Majzlan 2010). It is also significant that the assemblage includes minerals that are stable at ambient temperature ( $\sim 15\text{--}20^\circ\text{C}$ ) and very low relative humidity, such as rhomboclase, as well as phases that are characteristic of higher relative humidity, such

**Tab. 6** Hydrogen-bond geometry for the structure of bluelizardite

Bond	D–H	H...A	D...A	D–H...A
Ow19–H1...O8 <sup>xi</sup>	0.87 (3)	2.25 (3)	2.858 (3)	126.8 (19)
Ow20–H2...Cl <sup>i</sup>	0.87 (3)	2.52 (3)	3.335 (3)	155 (2)
Ow20–H3...Cl <sup>xiii</sup>	0.87 (2)	2.80 (3)	3.314 (3)	120 (3)
Ow19–H4...O15 <sup>i</sup>	0.87 (3)	1.99 (3)	2.862 (3)	177 (2)

Symmetry codes: (i)  $x, y-1, z$ ; (xi)  $x+1/2, y+1/2, z$ ; (xiii)  $-x+1/2, -y+5/2, -z+1$ .

Tab. 7 Bond-valence analysis for the structure of blueizardite

	U	S1	S2	S3	S4	Na1	Na2	Na3	Na4	Na5	Na6	Na7	Na8	ΣBV	H1	H2	H3	H4	ΣBV+H
O1		1.58					0.12×2↓		0.07				0.09	1.86					1.86
O2	0.48	1.44					0.15×2↓							2.07					2.07
O3		1.56						0.24	0.15				0.19	2.14					2.14
O4	0.41	1.45					0.15×2↓		0.11					2.12					2.12
O5			1.60					0.21	0.32					2.13					2.13
O6			1.52					0.16, 0.04			0.19		0.14	2.05					2.05
O7			1.55					0.17	0.17, 0.20					2.09					2.09
O8	0.56		1.46											2.02	0.17				2.19
O9				1.53				0.26			0.16		0.17	2.12					2.12
O10				1.62					0.25			0.13		2.00					2.00
O11				1.55								0.18	0.21	1.94					1.94
O12	0.53			1.34								0.05	0.15	2.07					2.07
O13					1.58	0.23×2↓						0.19		2.00					2.00
O14					1.53	0.25×2↓						0.17		2.13					2.13
O15					1.55					0.18				1.89				0.22	2.11
O16	0.56				1.38					0.16	0.18		0.08	2.02					2.02
O17	1.72											0.14		2.09					2.09
O18	1.72													1.92					1.92
Ow19							0.06×2↓	0.24			0.24			0.48	0.73			0.73	1.94
Ow20										0.16	0.23			0.39		0.73	0.73		1.85
Cl						0.11×2↓				0.44	0.14	0.12		0.81		0.11	0.06		0.98
ΣBV	5.98	6.03	6.13	6.04	6.04	1.18	0.97	1.32	1.02	1.19	1.14	1.06	0.95		0.90	0.84	0.79	0.95	

Notes: Values are expressed in valence units (vu). ΣBV = sum of bond-valences incident at the atom site; ΣBV + H = sum of the bond-valence with the contribution of the H-bonds; ×2↓ = multiplicity. U<sup>6+</sup>-O bond-valence parameters (r<sub>0</sub> = 2.045, b = 0.51) taken from Burns et al. (1997); Na<sup>+</sup>-O, Na<sup>+</sup>-Cl, S<sup>6+</sup>-O bond-valence parameters taken from Brown and Altermatt (1985), H<sup>+</sup>-O bond-valence parameters from Brown (2002) and H<sup>+</sup>-Cl bond-valence parameters from Malcherek and Schlitter (2007).

as chalcantite (Majzlan 2010 and references therein). However, this is not unreasonable, because these minerals form by evaporative processes at the surface of a rock with high relative porosity. There are no reliable data on the stability of uranyl sulfate minerals (including these newly described minerals from the Blue Lizard mine); however, some assumptions can be made using the bond-valence approach. An in-depth explanation of the basic principles and terminology of this approach can be found in Schindler and Hawthorne (2008). For borate aqueous species, Schindler and Hawthorne (2001) documented that the value of CDA, the *charge deficiency per anion* (called *average basicity* in their earlier papers), of the particular species correlates with the pH of the solution from which they formed. Therefore, it can be expected that minerals with structures having higher values of CDA will have formed from solutions of higher pH. This has been well documented by crystal-chemical and paragenetic observations for hydrated oxysalts (Schindler et al. 2000, 2006; Schindler and Hawthorne 2004, 2008). The minerals occurring in the general blueizardite association at the Blue Lizard mine with the CDA values of their structural units are provided in Tab. 8 [values for natrozippeite, copiapite, rhomboclase, metavoltine, römerite, siderontrite, ferrinatrite, kröhnkite and blöditite were taken from Schindler et al. (2006)] A wide range of CDA values is apparent in this list. We believe that these CDA values can be readily correlated with the observed paragenetic relations, in particular, for the recently-described uranyl sulfates. In general, a temporal development from low to high CDA values is inferred from growth relations, indicating a progressively higher pH in this assemblage. For example, meisserite (0.29 vu) is usually overgrown by belakovskiiite (0.36 vu), the latter apparently being the younger phase. In the typical association of meisserite and belakovskiiite, several additional

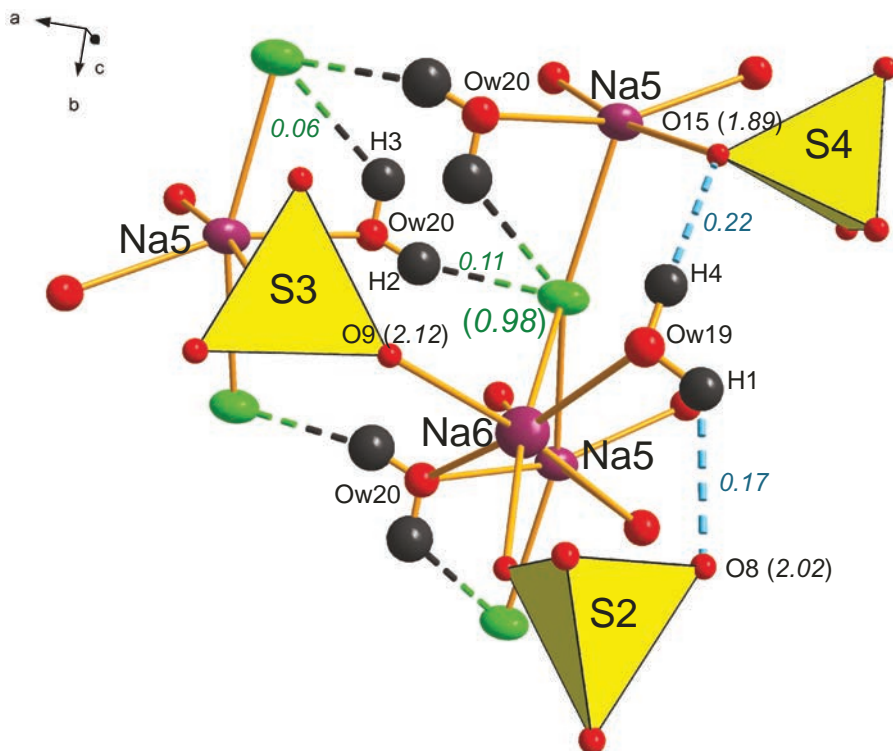


**Fig. 5** Hydrogen-bonding scheme in the bluelizardite structure. The bond-valence sums associated with anions without the contribution of H-bonds are black-labelled and printed in italics. The bond-valence associated with the particular H...O or H...Cl bond is shown in colour.

minerals were identified, including ferrinatrite (0.25 *vu*), sideronatrite (0.24 *vu*), metavoltine (0.22 *vu*), “blödites” (0.30 *vu*), kröhnkite (0.28 *vu*) and d’ansite-(Mn) (0.53 *vu*). In all observed cases, bluelizardite was inferred to be younger than all minerals except d’ansite-(Mn), which was clearly the last of these phases to form. The new Na-bearing uranyl sulfates are spatially isolated from other uranyl sulfates (natrozippeite, johannite and pseudojohannite), as well as from other minerals, either those characterized by low CDA (e.g. rhomboclase) or those with high CDA values

(e.g. halotrichite). Interestingly, the minerals containing structural units with low CDA values (copiapite, römerite,

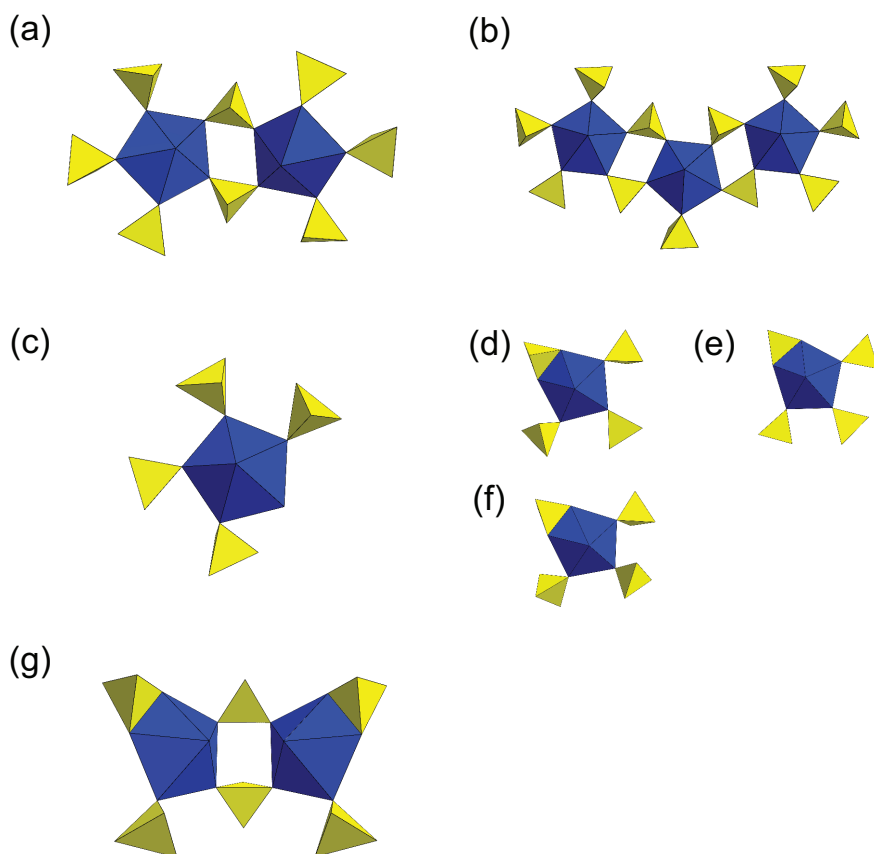


**Fig. 6** Structural units of selected uranyl-sulfates. **a** – The  $[(\text{UO}_2)_2(\text{SO}_4)_8]^{12-}$  cluster in the structure of bluelizardite. **b** – The infinite  $[(\text{UO}_2)(\text{SO}_4)_2]^+$  chain in the structure of meisserite (Plášil et al. 2013). **c** – The isolated  $[(\text{UO}_2)(\text{SO}_4)_4]^{6-}$  cluster in the structure of belakovskiiite (IMA 2013–075; Kampf et al. 2013). **d** – Isolated cluster in synthetic  $\text{Na}_6(\text{UO}_2)(\text{SO}_4)_4(\text{H}_2\text{O})_2$  (Hayden and Burns 2002a, b). **e** – Isolated cluster in synthetic  $\text{Na}_{10}[(\text{UO}_2)(\text{SO}_4)_4](\text{SO}_4)_2(\text{H}_2\text{O})_3$  (Burns and Hayden 2002). **f** – Isolated cluster in synthetic  $\text{KNa}_3[(\text{UO}_2)(\text{SO}_4)_4](\text{H}_2\text{O})$ . **g** – The cluster in synthetic  $\text{K}_4[(\text{UO}_2)(\text{SO}_4)_3]$  (Mikhailov et al. 1977).

**Tab. 8** Overview of the chemical composition of studied weathering association and the CDA values (in valence units, vu) of the structure units

Mineral	Composition	CDA [vu]
brochantite	$\text{Cu}(\text{SO}_4)(\text{OH})_6$	0.12
natrozippeite	$\text{Na}_3[(\text{UO}_2)_8(\text{SO}_4)_4\text{O}_5(\text{OH})_3](\text{H}_2\text{O})_{12}$	0.14
atacamite	$\text{Cu}_2\text{Cl}(\text{OH})_3$	0.15
copiapite	$\text{Fe}^{2+}\text{Fe}^{3+}_4(\text{SO}_4)_6(\text{OH})_2(\text{H}_2\text{O})_{20}$	0.16
johannite	$\text{Cu}[(\text{UO}_2)_2(\text{SO}_4)_2(\text{OH})_2](\text{H}_2\text{O})_8$	0.17
rhomboclase	$(\text{H}_3\text{O})\text{Fe}^{3+}(\text{SO}_4)_2(\text{H}_2\text{O})_3$	0.18
pseudojohannite	$\text{Cu}_3(\text{OH})_2[(\text{UO}_2)_4\text{O}_4(\text{SO}_4)_2](\text{H}_2\text{O})_{12}$	0.20
römerite	$\text{Fe}^{2+}\text{Fe}^{3+}_4(\text{SO}_4)_4(\text{H}_2\text{O})_{14}$	0.22
metavoltine	$\text{K}_2\text{Na}_6\text{Fe}^{3+}_6\text{Fe}^{2+}(\text{SO}_4)_{12}\text{O}_2(\text{H}_2\text{O})_{18}$	0.22
sideronatrite	$\text{Na}_2\text{Fe}^{3+}(\text{SO}_4)_2(\text{OH})(\text{H}_2\text{O})_3$	0.24
ferrinatrite	$\text{Na}_3\text{Fe}(\text{SO}_4)_3(\text{H}_2\text{O})_3$	0.25
kröhnkite	$\text{Na}_2\text{Cu}(\text{SO}_4)_2(\text{H}_2\text{O})_2$	0.28
meisserite	$\text{Na}_3(\text{UO}_2)(\text{SO}_4)_3(\text{SO}_3\text{OH})(\text{H}_2\text{O})$	0.29
blödite	$\text{Na}_2\text{Mg}(\text{SO}_4)_2(\text{H}_2\text{O})_4$	0.30
belakovskite	$\text{Na}_7(\text{UO}_2)(\text{SO}_4)_4(\text{SO}_3\text{OH})(\text{H}_2\text{O})_3$	0.36
bluelizardite	$\text{Na}_7(\text{UO}_2)(\text{SO}_4)_4\text{Cl}(\text{H}_2\text{O})_2$	0.37
tamarugite	$\text{NaAl}(\text{SO}_4)_2(\text{H}_2\text{O})_6$	0.50
halotrichite	$\text{Fe}^{2+}\text{Al}_2(\text{SO}_4)_4(\text{H}_2\text{O})_{22}$	0.50
chalcantite	$\text{Cu}(\text{SO}_4)(\text{H}_2\text{O})_3$	0.50
d'ansite-(Mn)	$\text{Na}_{21}\text{Mn}^{2+}(\text{SO}_4)_{10}\text{Cl}_3$	0.53

rhomboclase, pseudojohannite and natrozippeite) have a high molar proportion of  $\text{H}_2\text{O}$ . These phases probably formed directly from oversaturated solutions by precipitation and hydrolysis. Minerals with higher CDA values grew under more alkaline conditions, have a lower molar proportion of  $\text{H}_2\text{O}$  and probably crystallized from solutions by evaporation.

*Acknowledgements.* We are delighted to contribute this paper to the volume dedicated to our friend and colleague Jiří Čejka, on the occasion of his 85<sup>th</sup> birthday anniversary. Many thanks, Jiří, for your hard and careful scientific work and your friendship. We are grateful for help of Ladislav Lapčák (Institute of Chemical Technology, Prague) with the Raman spectroscopic measurements. The early version of the manuscript benefited from the constructive reviews of Frank Hawthorne and an anonymous reviewer. The editorial handling and care by Editor-in-chief is much appreciated. This work was financially supported by the Premium Academiae grant of the ASCR and by the post-doctoral grant of the GAČR no. 13-31276P to JP and by the John Jago Trelawney Endowment to the Mineral Sciences Department of the Natural History Museum of Los Angeles County.

*Electronic supplementary material.* Supplementary crystallographic data for this paper are available online at the Journal web site (<http://dx.doi.org/10.3190/jgeosci.159>).

## References

- AGILENT TECHNOLOGIES (2012) CrysAlis CCD and CrysAlis RED. Oxford Diffraction Ltd, Yarnton, Oxfordshire, UK
- BARTLETT JR, COONEY RP (1989) On the determination of uranium–oxygen bond lengths in dioxouranium(VI) compounds by Raman spectroscopy. *J Mol Struct* 193: 295–300
- BROWN ID (2002) *The Chemical Bond in Inorganic Chemistry. The Bond Valence Model*. Oxford University Press, Oxford, pp 1–288
- BROWN ID, ALTERMATT D (1985) Bond-valence parameters obtained from a systematic analysis of the inorganic crystal structure database. *Acta Cryst B* 41: 244–248
- BRUGGER J, MEISSER N, BURNS PC (2003) Contribution to the mineralogy of acid drainage of uranium minerals: marecottite and the zippeite-group. *Amer Miner* 88: 676–685
- BRUGGER J, WALLWORK KS, MEISSER N, PRING A, ONDRUŠ P, ČEJKA J (2006) Pseudojohannite from Jáchymov, Musonoï, and La Creusaz: a new member of the zippeite-group. *Amer Miner* 91: 929–936
- BURNS PC, HAYDEN LA (2002) A uranyl sulfate cluster in  $\text{Na}_{10}[(\text{UO}_2)(\text{SO}_4)_4](\text{SO}_4)_2 \cdot 3\text{H}_2\text{O}$ . *Acta Cryst C* 58: i121–i123
- BURNS PC, EWING RC, HAWTHORNE FC (1997) The crystal chemistry of hexavalent uranium: polyhedron geometries, bond-valence parameters, and polymerization of polyhedra. *Canad Mineral* 35: 1551–1570
- ČEJKA J (1999) Infrared spectroscopy and thermal analysis of the uranyl minerals. In: BURNS PC, EWING RC (eds) *Uranium: Mineralogy, Geochemistry and the Environment*. Mineralogical Society of America and Geochemical Society Reviews in Mineralogy and Geochemistry 38: pp 521–622
- FERNANDES HM, VEIGA LHS, FRANKLIN MR, PRADO VCS, TADDEI JF (1995) Environmental impact assessment of uranium mining and milling facilities; a study case at the Pocos de Caldas uranium mining and milling site, Brazil. In: ALLAN RJ, SALOMONS W (eds) *Heavy Metal Aspects of Mining Pollution and its Remediation*. Elsevier, Amsterdam, pp 161–173
- FINCH RJ, MURAKAMI T (1999) Systematics and paragenesis of uranium minerals. In: BURNS PC, EWING RC (eds) *Uranium: Mineralogy, Geochemistry and the Environment*. Mineralogical Society of America and Geochemical Society Reviews in Mineralogy and Geochemistry 38: pp 91–179
- GREVEL KD, MAJZLAN J (2011) Internally consistent thermodynamic data for metal divalent sulphate hydrates. *Chem Geol* 286: 301–306
- HAWTHORNE FC (2012) A bond-topological approach to theoretical mineralogy: crystal structure, chemical composition and chemical reactions. *Phys Chem Miner* 39: 841–874

- HAWTHORNE FC, SCHINDLER M (2008) Understanding the weakly bonded constituents in oxysalt minerals. *Z Kristallogr* 223: 41–68
- HAYDEN LA, BURNS PC (2002a) The sharing of an edge between a uranyl pentagonal bipyramid and sulfate tetrahedron in the structure of  $\text{KNa}_5[(\text{UO}_2)(\text{SO}_4)_4](\text{H}_2\text{O})$ . *Canad Mineral* 40: 211–216
- HAYDEN LA, BURNS PC (2002b) A novel uranyl sulfate cluster in the structure of  $\text{Na}_6(\text{UO}_2)(\text{SO}_4)_4(\text{H}_2\text{O})_2$ . *J Solid State Chem* 163: 313–318
- JOHNSON DB (2003) Chemical and microbiological characteristics of mineral spoils and drainage waters at abandoned coal and metal mines. *Water Air Soil Pollut: Focus* 3: 47–66
- JOHNSON DB, HALLBERG KB (2005) Acid mine drainage remediation options: a review. *Sci Total Environ* 338: 3–14
- KAMPF AR, PLÁŠIL J, KASATKIN AV, MARTY J (2013) Belakovskiiite, IMA 2013-075. *CNMNC Newsletter* 18, December 2013, page 3252. *Mineral Mag* 77: 3249–3258
- KASATKIN AV, NESTOLA F, PLÁŠIL J, MARTY J, BELAKOVSKIY DI, AGAKHANOV AA, MILLS SJ, PEDRON D, LANZA A, FAVARO M, BIANCHIN S, LYKOVA IS, GOLIÁŠ V, BIRCH WD (2013) Manganoblödite,  $\text{Na}_2\text{Mn}(\text{SO}_4)_2 \cdot 4\text{H}_2\text{O}$ , and cobaltoblödite,  $\text{Na}_2\text{Co}(\text{SO}_4)_2 \cdot 4\text{H}_2\text{O}$ : two new members of the blödite group from the Blue Lizard mine, San Juan County, Utah, USA. *Mineral Mag* 77: 367–383
- KRIVOVICHEV SV, BURNS PC (2001) Crystal chemistry of uranyl molybdates. III. New structural themes in  $\text{Na}_6[(\text{UO}_2)_2\text{O}(\text{MoO}_4)_4]$ ,  $\text{Na}_6[(\text{UO}_2)(\text{MoO}_4)_4]$  and  $\text{K}_6[(\text{UO}_2)_2\text{O}(\text{MoO}_4)_4]$ . *Canad Mineral* 39: 197–206
- KRIVOVICHEV SV, BURNS PC (2003) Crystal chemistry of uranyl molybdates. VIII. Crystal structures of  $\text{Na}_3\text{Ti}_3[(\text{UO}_2)(\text{MoO}_4)_4]$ ,  $\text{Na}_{13-x}\text{Ti}_{3+x}[(\text{UO}_2)(\text{MoO}_4)_{3.4}(\text{H}_2\text{O})_{6+x}]$  ( $x = 0.1$ ),  $\text{Na}_3\text{Ti}_5[(\text{UO}_2)(\text{MoO}_4)_3]_2(\text{H}_2\text{O})_3$  and  $\text{Na}_2[(\text{UO}_2)(\text{MoO}_4)_2](\text{H}_2\text{O})_4$ . *Canad Mineral* 41: 707–719
- KRIVOVICHEV SV, PLÁŠIL J (2013) Mineralogy and Crystallography of Uranium. In: BURNS PC, SIGMON GE (eds) *Uranium: From Cradle to Grave*. Mineralogical Association of Canada Short Courses 43: pp 15–119
- LIBOWITZKY E (1999) Correlation of O–H stretching frequencies and O–H...O hydrogen bond lengths in minerals. *Monatsh Chem* 130: 1047–1059
- MAJZLAN J (2010) Advances and gaps in the knowledge of thermodynamics and crystallography of acid mine drainage sulfate minerals. *Chimia* 64: 699–704
- MALCHEREK T, SCHLÜTER J (2007)  $\text{Cu}_3\text{MgCl}_2(\text{OH})_6$  and the bond-valence parameters of the OH–Cl bond. *Acta Cryst B* 63: 157–160
- MIKHAILOV YU N, GORBUNOVA YUE, KOKH LA, KUZNETSOV VG, GREVTSEVA TG, SOKOL SK, ELLERT GV (1977) Synthesis and crystal structure of potassium trisulfatouranyl-ate  $\text{K}_4(\text{UO}_2(\text{SO}_4)_3)$ . *Koord Khim* 3: 508–513
- ONDRUŠ P, VESELOVSKÝ F, HLOUŠEK J, SKÁLA R, VAVŘÍN I, FRÝDA J, ČEJKA J, GABAŠOVÁ A (1997) Secondary minerals of the Jáchymov (Joachimsthal) ore district. *J Czech Geol Soc* 42: 3–76
- ONDRUŠ P, VESELOVSKÝ F, GABAŠOVÁ A, DRÁBEK M, DOBEŠ P, MALÝ K, HLOUŠEK J, SEJKORA J (2003) Ore-forming processes and mineral parageneses of the Jáchymov ore district. *J Czech Geol Soc* 48: 157–192
- OSZLÁNYI G, SÜTŐ A (2004) *Ab initio* structure solution by charge flipping. *Acta Cryst A* 60: 134–141
- OSZLÁNYI G, SÜTŐ A (2008) The charge flipping algorithm. *Acta Cryst A* 64: 123–134
- PALATINUS L (2013) The charge flipping algorithm in crystallography. *Acta Cryst B* 69: 1–16
- PALATINUS L, CHAPUIS G (2007) Superflip – a computer program for the solution of crystal structures by charge flipping in arbitrary dimensions. *J Appl Cryst* 40: 451–456
- PALATINUS L, VAN DER LEE A (2008) Symmetry determination following structure solution in *P1*. *J Appl Cryst* 41: 975–984
- PETŘÍČEK V, DUŠEK M, PALATINUS L (2006) Jana2006. The crystallographic computing system. Institute of Physics, Prague, Czech Republic. Accessed on January 21, 2014, at <http://jana.fzu.cz>
- PLÁŠIL J, BUIXADERAS E, ČEJKA J, SEJKORA J, JEHLIČKA J, NOVÁK M (2010) Raman spectroscopic study of the uranyl sulphate mineral zippeite: low wavenumber and U–O stretching regions. *Anal Bioanal Chem* 397:2703–2715
- PLÁŠIL J, DUŠEK M, NOVÁK M, ČEJKA J, ČISAŘOVÁ I, ŠKODA R (2011a) Sejkoraite-(Y), a new member of the zippeite group containing trivalent cations from Jáchymov (St. Joachimsthal), Czech Republic: description and crystal structure refinement. *Amer Miner* 96: 983–991
- PLÁŠIL J, MILLS SJ, FEJFAROVÁ K, DUŠEK M, NOVÁK M, ŠKODA R, ČEJKA J, SEJKORA J (2011b) The crystal structure of natural zippeite,  $\text{K}_{1.85}\text{H}^{+}_{0.15}[(\text{UO}_2)_4\text{O}_2(\text{SO}_4)_2(\text{OH})_2](\text{H}_2\text{O})_4$ , from Jáchymov, Czech Republic. *Canad Mineral* 49: 1089–1103
- PLÁŠIL J, HLOUŠEK J, VESELOVSKÝ F, FEJFAROVÁ K, DUŠEK M, ŠKODA R, NOVÁK M, ČEJKA J, SEJKORA J, ONDRUŠ P (2012) Adolfpateraite,  $\text{K}(\text{UO}_2)(\text{SO}_4)(\text{OH})(\text{H}_2\text{O})$ , a new uranyl sulphate mineral from Jáchymov, Czech Republic. *Amer Miner* 97: 447–454
- PLÁŠIL J, KAMPF AR, KASATKIN AV, MARTY J, ŠKODA R, SILVA S, ČEJKA J (2013a) Meisserite,  $\text{Na}_5(\text{UO}_2)(\text{SO}_4)_3(\text{SO}_3\text{OH})(\text{H}_2\text{O})$ , a new uranyl sulfate mineral from the Blue Lizard mine, San Juan County, Utah, USA. *Mineral Mag* 77: 2975–2988
- PLÁŠIL J, FEJFAROVÁ K, ŠKODA R, DUŠEK M, MARTY J, ČEJKA J (2013b) The crystal structure of magnesiozippeite,  $\text{Mg}[(\text{UO}_2)_2\text{O}_2(\text{SO}_4)](\text{H}_2\text{O})_{3.5}$ , from East Saddle Mine, San Juan County, Utah (U.S.A.). *Mineral Petrol* 107: 211–219
- SCHINDLER M, HAWTHORNE FC (2001) A bond-valence approach to the structure, chemistry and paragenesis of hydroxy-hydrated oxysalt minerals. III. Paragenesis of borate minerals. *Canad Mineral* 39: 1257–1274

SCHINDLER M, HAWTHORNE FC (2004) A bond-valence approach to the uranyl-oxide hydroxy-hydrate minerals: chemical composition and occurrence. *Canad Mineral* 42: 1601–1627

SCHINDLER M, HAWTHORNE FC (2008) The stereochemistry and chemical composition of interstitial complexes in uranyl-oxysalt minerals. *Canad Mineral* 46: 467–501

SCHINDLER M, HAWTHORNE FC, BAUR WH (2000) A crystal chemical approach to the composition and occurrence of vanadium minerals. *Canad Mineral* 38: 1443–1456

SCHINDLER M, HUMINICKI DMC, HAWTHORNE FC (2006) Sulfate minerals. I. Bond topology and chemical composition. *Canad Mineral* 44: 1403–1429